Cooperative Photometallobiocatalysis: Nonheme Fe Enzyme-Catalyzed Enantioconvergent Radical Decarboxylative Azidation, Thiocyanation and Isocyanation of Redox-Active Esters

Liu-Peng Zhao,[a] Ken Lin,[a] Pei-Pei Xie,[b] Huichong Liu,[a] Hengye Xiang,[b] Xin Liu,[a] Yunlong Zhao,[a] Peng Liu*[b] and Yang Yang*[a],[c]

[a] L.-P. Zhao, K. Lin, H. Liu, Y. Zhao and Y. Yang
Department of Chemistry and Biochemistry, University of California Santa Barbara, Santa Barbara, California 93106, USA
E-mail: yang@chem.ucsb.edu

[b] P.-P. Xie, H. Xiang, and P. Liu
Department of Chemistry, University of Pittsburgh, Pittsburgh, Pennsylvania 15260, USA
E-mail: pengliu@pitt.edu

[c] Y. Yang
Biomolecular Science and Engineering (BMSE) Program, University of California Santa Barbara, Santa Barbara, California 93106, USA
E-mail: yang@chem.ucsb.edu

Supporting information for this article is given via a link at the end of the document.

Abstract: Cooperative catalysis with an enzyme and a small-molecule photocatalyst has very recently emerged as a potentially general activation mode to advance novel biocatalytic reactions with synthetic utility. Herein, we report cooperative photobiocatalysis involving an engineered nonheme Fe enzyme and a tailored photoredox catalyst as a unifying strategy for the catalytic enantioconvergent decarboxylative azidation, thiocyanation and isocyanation of redox-active esters via a radical mechanism. Through the survey and directed evolution of nonheme Fe enzymes, we repurposed and further evolved metapyrocatechase (MPC), a nonheme Fe extradiol dioxygenase not previously studied in new-to-nature biocatalysis, for the enantioselective C–N_3, C–SCN and C–NCO bond formation through a radical rebound mechanism with an enzymatic Fe–X intermediate (X = N_3, NCS, and NCO). A range of primary, secondary and tertiary alkyl radical precursors were effectively converted by our engineered MPC, allowing the syntheses of organic azides, thiocyanates and isocyanates with good to excellent enantiocontrol. Further chemical derivatization of these products furnished valuable compounds including enantioenriched amines, triazoles, ureas and SCF_3-containing products. Computational studies via DFT and MD simulations shed light on the mechanism as well as the binding poses of the alkyl radical intermediate in the enzyme active site and the π-facial selectivity in the enantiodetermining radical rebound. Overall, cooperative photometallobiocatalysis with nonheme Fe enzymes provides a means to develop challenging asymmetric radical transformations eluding small-molecule catalysis.

Introduction

The past several years have witnessed exciting developments in the field of stereoselective radical biocatalysis.[1-2] Guided by the fundamental principles of organic and transition-metal chemistry, various organic cofactor[2-7] and metallocofactor[8-11] -dependent enzymes were repurposed to catalyze free radical-mediated asymmetric transformations previously unknown in enzymology, allowing the achievement of challenging stereocontrol over free radical intermediates, many of which had previously eluded small-molecule catalyst systems.[12] In the early stages of this effort, the central doctrine in biocatalytic radical reaction design emphasized that the key radical intermediate must be generated within the enzyme's active site, often through the involvement of a redox-active cofactor and/or substrate-cofactor charge transfer complex.[8-9,13] In these processes, the binding and activation of the radical precursor with the enzyme precede radical initiation. While this strategy has proven tremendously successful and culminated in an astonishing array of useful biocatalytic radical reactions,[2] it poses limitations for the types of enzymes that could be used for rational radical reaction design.

In 2023, through the cooperative interactions between the biocatalyst and the small-molecule photosensitizer, our group reported the first use of pyridoxal 5'-phosphate (PLP)-dependent enzymes to catalyze asymmetric intermolecular radical C–C couplings which were not previously known in either organic chemistry or biochemistry.[6a] In this process, the key reactive radical intermediate forms photocatalytically outside the enzyme active site and then travel into the active site, likely guided by hydrophobic interactions with the enzyme pocket, for productive bond formation with an enzymatic intermediate.[6] By separating radical generation from enzymatic substrate activation, this new mechanism holds the potential to be generalized to diverse enzyme families, including those lacking a redox-active cofactor. Furthermore, external radical generation from a discrete photoredox[14] cycle enables biocatalytic radical transformations to be carried out in an intermolecular sense, which remains a currently unmet challenge for several biocatalytic activation modes involving radical initiation within the active site. [8-9]

Cognizant of the tremendous potential of external radical generation via cooperative catalysis for developing new biocatalytic radical reactions, we sought to generalize this strategy to other enzyme families. Due to our ongoing focus on the engineering of heme[8] and nonheme[9c] Fe enzymes for enantioselective radical processes, we questioned whether *cooperative photometallobiocatalysis* could be achieved with nonheme Fe enzymes to allow for asymmetric carbon–heteroatom bond formation via a radical mechanism. Inspired by pioneering studies illuminating the reactivity of nonheme Fe(III)–X (X = halogen,[9b,c,15] N_3,[9a,d,16] and NCS[17]) with both Fe enzymes[18] and small-molecule model Fe complexes,[19-20] we posited that the externally formed free radical intermediate could be intercepted by an enzymatic Fe(III)–X species (X = N_3, NCS and NCO), thereby providing a unifying strategy for catalytic asymmetric azidation, thiocyanation and isocyanation of open-shell intermediates. Despite extensive recent studies on transition-metal catalyzed azidation[20] and related radical functionalization reactions[21] in the arena of synthetic organic chemistry, to date, catalytic asymmetric radical thiocyanation[22] and isocyanation[23] has remained unknown with chiral small-molecule transition-metal catalysts. Thus, the development of nonheme Fe enzyme-catalyzed asymmetric radical rebound reactions will provide a new platform to address this challenge.

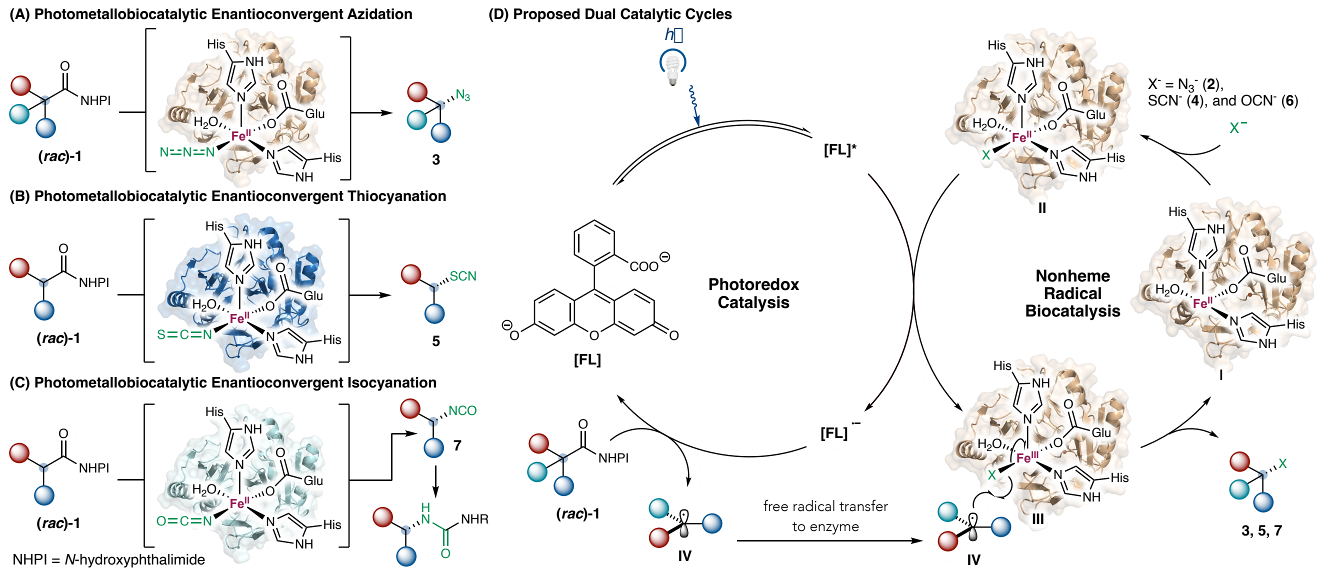

Scheme 1. Nonheme Fe enzyme-catalyzed enantioconvergent decarboxylative radical azidation, thiocyanation and isocyanation of redox-active esters enabled by cooperative photometallobiocatalysis. PyMol illustration of metapyrocatechase (MPC), a nonheme Fe extradiol dioxygenase, is made from PDB ID: 1MPY. FL: fluorescein, a photocatalyst. The red sphere is an aryl substituent.

Our proposed cooperative photometallobiocatalytic asymmetric C–N/C–S bond formation involves two discrete catalytic cycles. For clarity, photometallobiocatalytic enantioconvergent azidation of redox-active esters is illustrated as an example (Scheme 1) for this class of enantioselective radical rebound processes. In the photoredox cycle, we envisioned that a proper photosensitizer such as fluorescein (FL) would oxidize the Fe(II) species in its excited state ($FL^*/FL^{\bullet-}$ = +0.77 V *versus* SCE in MeOH)[14d,24] to afford the radical anion state $FL^{\bullet-}$. This radical anion ($FL^{\bullet-}$) and related photosensitizer radical anions in their ground state is a potent single electron reductant and is known to promote reductive radical generation with *N*-hydroxyphthalimide esters.[7a,b] In this single electron transfer process, the radical anion $FL^{\bullet-}$ would also be converted back to the neutral photosensitizer FL, thereby completing the photoredox cycle. Concurrently, in the nonheme biocatalytic cycle, we postulated that the enzymatic iron center would stay in an azide-bound form due to the strong binding affinity of N_3^- towards Fe.[16a,19a] This enzymatic Fe(II)–N_3 species would be rapidly oxidized by the excited state photosensitizer FL*, giving rise to the key Fe(III)–N_3 intermediate. We hypothesized that driven by hydrophobic interactions, the photoredox-generated radical intermediate formed outside the enzyme pocket would enter the active site and engage the protein-bound Fe(III)–N_3 intermediate, leading to the formation of enantioenriched organic azide product via a rebound mechanism. Meanwhile, this radical rebound step would also return Fe(III) to Fe(II) and complete the enzymatic cycle.

We reasoned that through directed evolution, we could engineer highly stereoselective nonheme Fe enzymes to allow the enantioconvergent decarboxylative azidation of racemic redox-active esters, leading to valuable secondary- and tertiary-alkyl azides in a highly enantioenriched form. Furthermore, as nonheme Fe enzymes could potentially bind other anions including thiocyanate (SCN^-) and cyanate (OCN^-), we envisioned that through the identification and engineering of suitable nonheme Fe enzyme scaffolds, we could generalize this strategy and accomplish enantioselective radical thiocyanation and isocyanation. Due to the synthetic versatility of organic azides, thiocyanates and isocyanates and a variety of previously established transformations associated with these building blocks, our photometallobiocatalytic azidation, thiocyanation and isocyanation methods would provide a powerful means to the asymmetric synthesis of valuable molecular entities.

Herein, we describe the successful implementation of this cooperative photometallobiocatalysis design through the repurposing and directed evolution of metapyrocatechase (MPC), a nonheme Fe extradiol dioxygenase.[25] As a nonheme Fe enzyme that does not require a co-substrate such as a-ketoglutarate for its native function, MPC and related extradiol dioxygenases have not yet been studied in new-to-nature biocatalysis. During the submission of this manuscript, elegant related study on the engineering of 4-hydroxyphenylpyruvate dioxygenase (HPPD) from the Huang group appeared in the literature.[26] We note that our MPC is phylogenetically distal and functionally distinct to HPPD with a sequence similarity (percent identity) of only 16%. Additionally, the organic azide and thiocyanate products prepared from our engineered MPC are the *opposite enantiomer* of those obtained with Huang's HPPD.[26] Furthermore, our MPC-catalyzed asymmetric isocyanation with OCN^- for unsymmetrical urea synthesis remains elusive with other nonheme Fe enzymes in photobiocatalysis.

Results and Discussion

Discovery and directed evolution of nonheme Fe enzymes for cooperative photometallobiocatalytic enantioconvergent decarboxylative azidation

We initiated this investigation by evaluating an in-house collection of ca. 200 nonheme Fe enzymes and enzyme variants generated from our prior study[9c] for the targeted asymmetric decarboxylative azidation of redox-active *N*-hydroxyphthalimide esters using fluorescein[8d] as the photocatalyst (Table 1). Using racemic *N*-hydroxyphthalimide esters **1a** as the model substrate, in the prescence of 5 mol% fluorescein, 5 mol% added $(NH_4)_2Fe(II)(SO_4)_2$ (Mohr's salt) and 3.0 equiv NaN_3 (**2**), the use of 1 mol% 2-hydroxypropylphosphonate epoxidase (HPPE) from *Streptomyces wedmorensis* (Uniprot ID: Q56185)[27] did not lead to the desired organic azide product **3a** (Table 1, entry 1). When 4-hydroxyphenylpyruvate dioxygenase (HPPD) from *Streptomyces avermitilis* (Uniprot ID: Q53586)[28] was used, organic azide **3a** formed in 11% yield and 33:67 enantiomeric ratio (e.r., entry 2). Quercetin 2,3-dioxygenase(QueD) from *Bacillus subtilis* (Uniprot ID: P42106)[29] was also found to be a good nonheme Fe enzyme candidate for this transformation, furnishing **3a** in 8% yield and 45:55 e.r. (entry 3). 1-Aminocyclopropane-1-carboxylate oxidase (ACCO) from *Petunia hydrida* (Uniprot ID: Q08506)[30], a nonheme Fe enzyme we previously engineered for C–F bond formation, was also effective, albeit with lower activity and enantioselectivity (4% yield and 55:45 e.r., entry 4). Other nonheme Fe enzymes, including biphenyl-2,3-diol 1,2-dioxygenase (BDDO) from *Pseudomonas aeruginosa* (Uniprot ID: Q79F01)[31] and an ergothioneine biosynthetic enzyme EgtB (a hercynine oxygenase) from *Mycolicibacterium thermoresistibile* (Uniprot ID: G7CFI3)[32] provided **3a** in 4% yield, 75:25 e.r. (entry 5) and 7% yield, 46:54 e.r., respectively. Finally, metapyrocatechase (MPC) form *Pseudomonas putida* (Uniprot ID: P06622), an extradiol dioxygenase whose native function is to convert catechol into 2-hydroxy-6-oxohexa-2,4-dienoate under O_2 dependent conditions, provided the secondary alkyl azide product (**3a**) with the highest activity and enantioselectivity (28% yield, 77:23 e.r., entry 6). In light of the substantially higher initial activity of *Pp*MPC relative to all the other nonheme Fe enzymes we examined, MPC was selected as the template for further enzyme engineering. A detailed phylogenetic analysis of nonheme Fe enzymes described in Table 1 can be found in Figure S5.

Table 1. Discovery of photometallobiocatalytic enantioconvergent decarboxylative azidation: evaluation of in-house collection of nonheme Fe enzymes.[a]

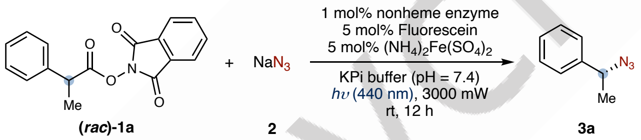

entry	nonheme Fe enzyme	Uniprot ID	yield of **3a**	e.r. of **3a**
1	*Sw*HPPE	Q56185	<1%	–
2	*Sa*HPPD	Q53586	11%	33:67
3	*Bs*QueD	P42106	8%	45:55
4	*Pa*BDDO	Q79F01	4%	75:25
5	*Ph*ACCO	Q08506	4%	55:45
6	*Mt*EgtB	G7CFI3	7%	46:54
7	***Pp*MPC**	**P06622**	**28%**	**77:23**

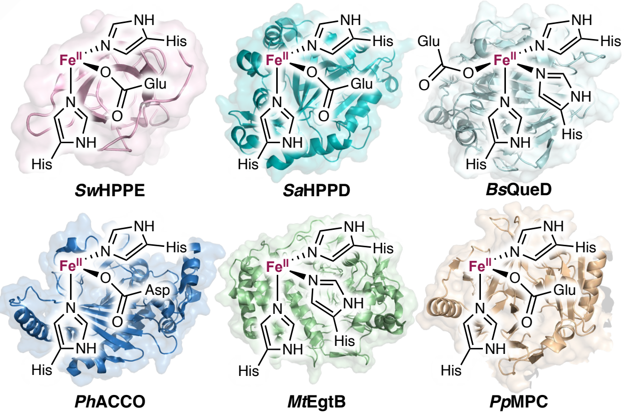

[a] Reaction conditions: **1a** (6.67 mM), **2** (20.0 mM, 3.0 equiv), 1.0 mol% nonheme Fe enzyme (66.7 μM), 5 mol% fluorescein sodium salt (0.33 mM), 5 mol% $(NH_4)_2Fe(II)(SO_4)_2$ (0.33 mM), *hν* (440 nm), 200 mM KPi buffer, pH = 7.4, rt, 12 h.

Next, we performed further reaction condition optimization to improve the efficiency of this dual photobiocatalytic azidation with wild-type (wt) *Pp*MPC (Table 2). A wide range of transition-metal and organic photoredox catalysts was evaluated. It was found that transition-metal-based photosensitizers were inferior to organic dyes. For example, the use of 3 mol% $[Ru(bpy)_3]Cl_2$ in lieu of fluorescein only furnished **3a** in1% yield and 74:26 e.r. (Table 2, entry 2). The employment of *fac*-$Ir(ppy)_3$ only led to trace amount of **3a** (<1% yield, 66:34 e.r., entry 3). Among organic photoredox catalysts, Fukuzumi's acridinium salt[33] showed a low degree of activity (2% yield, 66:34 e.r., entry 4). Rhodamine dyes such as rhodamine B (RhB) exhibited improved activity, resulting in the formation of **3a** in 12% yield and 76:24 e.r. (entry 5). Organic photosensitizers from the fluorescein family in general displayed the highest activity. For example, Eosin Y was found to be able to facilitate the formation of **3a** in 21% yield and 77:23 e.r. (entry 6). After surveying additional organic photocatalysts (see Table S2 in the SI for full details), the structurally simplest fluorescein remained the best photocatalyst (entry 1). The use of 3 mol% added ferrous Mohr's salt $(NH_4)_2Fe(II)(SO_4)_2$ was critical to achieving good efficiency, as replacing Mohr's salt with ferric salt $(NH_4)Fe(III)(SO_4)_2$ provided much lower efficiency (24% yield, entry 7). Omitting $(NH_4)_2Fe(II)(SO_4)_2$ under the standard reaction conditions led to 21% yield of **3a** along with 77:23 e.r. (entry 8). Together, these results are consistent with previous biochemical studies showing MPC's strong binding affinity towards Fe(II) and attenuated binding affinity towards Fe(III)[25a]. Irradiation at 525 nm using green LED led to reduced yield (24%) of **3a** under otherwise identical reaction conditions (entry 9). The use of *N*-hydroxytetrachlorophthalimide ester **1a'** previously used in radical coupling reactions[34] in place of **1a** also resulted in drastically reduced yield of **3a** (2%, entry 10). Finally, omitting the nonheme enzyme *Pp*MPC (entry 11), the photocatalyst fluorescein (entry 12) and visible light source (440 nm, entry 13) under the standard reaction conditions led to no product **3a** formation, confirming the dual photometallobiocatalytic nature of the present transformation.

Table 2. Reaction condition optimization for photometallobiocatalytic enantioconvergent decarboxylative azidation: evaluation of photocatalysts and other parameters.[a]

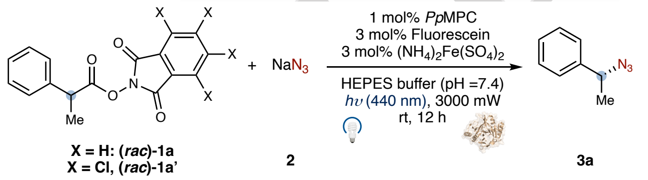

entry	deviation from standard conditions	yield of 3a	e.r. of 3a
1	none	32%	77:23
2	$[Ru(bpy)_3]Cl_2$ instead of fluorescein	1%	74:26
3	*fac*-$Ir(ppy)_3$ instead of fluorescein	<1%	66:34
4	acridinium instead of fluorescein	2%	66:34
5	RhB instead of fluorescein	12%	76:24
6	Eosin Y instead of fluorescein	21%	77:23
7	$(NH_4)Fe(III)(SO_4)_2$ instead of $(NH_4)_2Fe(II)(SO_4)_2$	24%	77:23
8	no $(NH_4)_2Fe(II)(SO_4)_2$	21%	77:23
9	$h\nu$ (525 nm)	24%	76:24
10	**(*rac*)-1a'** instead of **(*rac*)-1a**	2%	77:23
11	no *Pp*MPC	0	–
12	no fluorescein	0	–
13	no $h\nu$	0	–

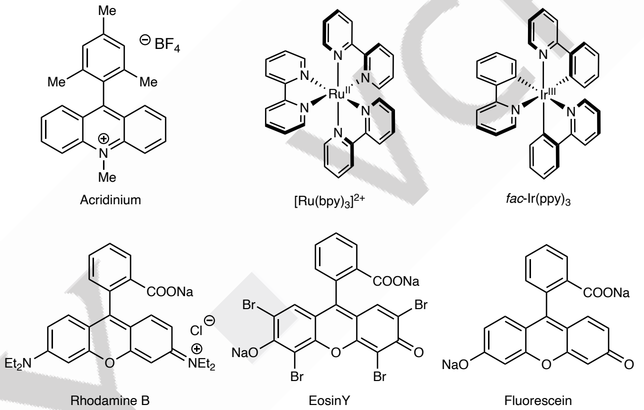

[a] Reaction conditions: **1a** (6.67 mM), **2** (20.0 mM, 3.0 equiv), 1.0 mol% wt *Pp*MPC (66.7 μM), 3 mol% fluorescein sodium salt (0.20 mM), 3 mol% $(NH_4)_2Fe(II)(SO_4)_2$ (0.20 mM), $h\nu$ (440 nm), 200 mM KPi buffer, pH = 7.4, rt, 6 h.

With chemically optimal conditions in hand, we carried out the directed evolution of *Pp*MPC to further improve its activity and enantioselectivity in this asymmetric decarboxylative azidation (Table 3). To aid in this enzyme engineering campaign, we first build a substrate tunnel model using CAVER[35] (Figure 1). Due to the tetrameric aggregation state of *Pp*MPC,[36] the substrate tunnel with the highest priority score identified by CAVER has its entrance blocked by the neighboring polypeptide chain. After careful examination, the substrate tunnel revealed by CAVER with the second highest priority score was consistent with previous structural studies with *Pp*MPC.[25a] It was thus identified as the key channel for the radical intermediate to enter the active site and approach the nonheme Fe center. As a notable feature, a series of hydrophobic amino acid residues including L155, V188, F191, I204, L248, L287, I291, F302 and M303 flanking the entrance of this substrate tunnel, thus creating a hydrophobic lid of the substrate binding pocket.[25]

Table 3. Directed evolution of *Pp*MPC for photometallobiocatalytic enantioconvergent decarboxylative azidation.[a]

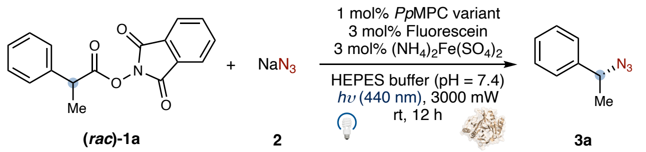

(*rac*)-**1a**   **2**   **3a**

entry	*Pp*MPC variant	yield of **3a**	e.r. of **3a**
1	*Pp*MPC	30%	77:23
2	*Pp*MPC I291L	56%	91:9
3	*Pp*MPC I291L L155F	72%	97.5:2.5
4	*Pp*MPC I291L L155F (0.25 mol%)	57%	97.5:2.5
5	***Pp*MPC I291L L155F F302Y (*Pp*MPC azidase)**	**74%**	**99.5:0.5**
6	*Pp*MPC I291L L155F F302Y (**0.25 mol%**)	62%	99.5:0.5

[a] Reaction conditions: **1a** (6.67 mM), **2** (20.0 mM, 3.0 equiv), 0.25–1.0 mol% *Pp*MPC variant (16.7–66.7 μM), 3 mol% fluorescein sodium salt (0.20 mM), 3 mol% $(NH_4)_2Fe(II)(SO_4)_2$ (0.20 mM), $h\nu$ (440 nm), 10 mM HEPES buffer, pH = 7.4, rt, 6 h.

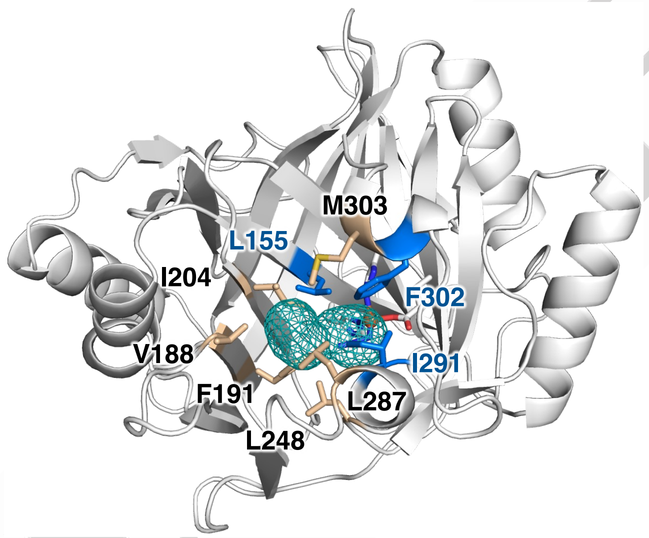

Figure 1. *Pp*MPC's substrate tunnel identified by CAVER[35] and hydrophobic residues flanking the tunnel entrance. PyMol illustration of MPC is made from PDB ID: 1MPY. Beneficial mutation sites are colored in marine. Other hydrophobic residues are colored in wheat.

Equipped with this understanding, we used site-saturation mutagenesis (SSM) and screening to direct the evolution of *Pp*MPC by targeting residues from the substrate tunnel (Table 3). We first focused on residues from the substrate tunnel which are closer to the nonheme Fe center and then turned our attention to residues further outside closer to the entrance of the substrate tunnel. To facilitate this engineering campaign, we assembled an in-house setup for high throughput photochemistry with temperature control. Nonheme enzyme expression was carried out in 24-well plate and for each SSM library constructed using the 22c trick method[37], 88 clones per library were selected for screening. In the first round of SSM and evaluation, an isoleucine (I) to leucine (L) displacement at residue 291 (I291L) was found to be a key beneficial mutation, resulting in almost two-fold enhancement in activity and significantly better enantioselectivity (Table 3, entries 1 and 2). In subsequent enzyme engineering, L155F was discovered as another important mutation, allowing the further enhancement of both the yield and enantioselectivity of azide product **3a** (72% yield, 97.5:2.5 e.r., entry 3). A final round of engineering afforded triple mutant *Pp*MPC I291L L155F F302Y. At 1 mol% loading of this triple mutant enzyme, **3a** formed in 74% yield and 99.5:0.5 e.r. (entry 5). Furthermore, by further lowering the enzyme loading to 0.25 mol%, **3a** could be prepared in a comparable yield and identical enantioselectivity (62% yield and 99.5:0.5 e.r., entry 6), indicating the enhanced efficiency and enantiocontrol of this final *Pp*MPC azidase variant. The absolute stereochemistry of **3a** was determined by comparison with authentic samples prepared by other methods (see the SI for details).

With the newly evolved nonheme Fe azidase *Pp*MPC I291L L155F F302Y, we examined its substrates scope (Table 4). *N*-hydroxyphthalimide esters with a methyl substituent attached to the *ortho*- (**3b**), *meta*- (**3c**) and *para*- (**3d**) positions of the aromatic ring were readily accommodated by the *Pp*MPC triple mutant, giving rise to the corresponding secondary alkyl azide products with excellent enantioselectivity. Additionally, halogen substituents including a fluorine (**3e**), a chlorine (**3f**), and a bromine (**3g**) were also compatible with this process. The availability of a halogen functional group handle permitted further functionalization of the aromatic ring via cross-coupling technologies.[38] Furthermore, a wide range of electron-withdrawing substituents, including a *para*-trifluoromethyl (**3h**), a *para*-trifluoromethoxy (**3i**), a *meta*-methoxy (**3k**) and a *meta*-cyano (**3l**) group, were readily tolerated by this radical azidation reaction. Sensitive functional groups such as a 4-methylthio (**3k**) and a cyano (**3l**) as well as heterocycles including thiophenes (**3n** and **3q**) and a pyridine (**3o**) were also readily accommodated. Furthermore, redox-active esters bearing an extended α-aliphatic chain including an α-ethyl (**3p**) and an α-propyl (**3q**) could also be transformed with excellent yield and varying enantioselectivity. Cyclic *N*-hydroxyphthalimide esters such as an indane moiety (**3r** and **3t**) and a tetrahydronaphthalene moiety (**3s**) were also accepted by our evolved dual photometallobiocatalytic system, giving rise to the corresponding cyclic organic azide products with good enantiocontrol. Finally, without additional enzyme engineering, racemic tertiary alkyl radical precursors (**3t**) could also be applied, delivering the corresponding tertiary alkyl azide product with modest enantioselectivity. Together, these results demonstrate the potential utility of this nonheme Fe enzyme-catalyzed radical azidation in preparing enantioenriched products.

Table 4. Substrate scope of photometallobiocatalytic enantioconvergent decarboxylative azidation of redox-active esters.[a]

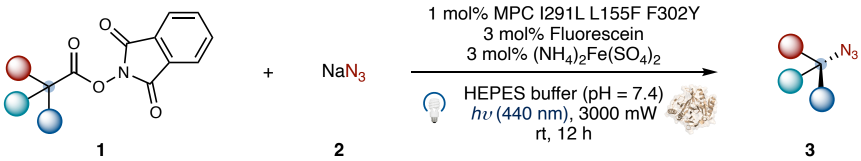

1 2 3

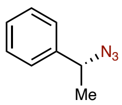

3a
74 ± 1% yield
99.5:0.5 e.r.

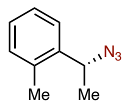

3b
66 ± 1% yield
93:7 e.r.

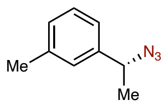

3c
68 ± 1% yield
99:1 e.r.

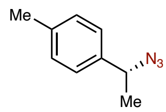

3d
69 ± 1% yield
98:2 e.r.

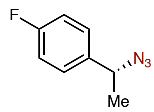

3e
68 ± 1% yield
99.5:0.5 e.r.

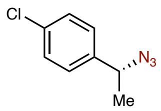

3f
55 ± 2% yield
99.5:0.5 e.r.

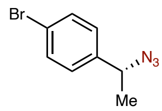

3g
41 ± 3% yield
99:1 e.r.

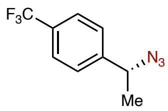

3h[b]
58 ± 1% yield
99.5:0.5 e.r.

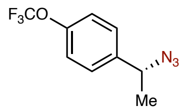

3i
54 ± 1% yield
99.5:0.5 e.r.

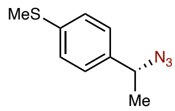

3j
22 ± 1% yield
84:16 e.r.

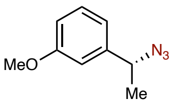

3k
74 ± 2% yield
99:1 e.r.

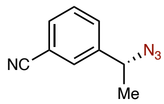

3l
52 ± 2% yield
99.5:0.5 e.r.

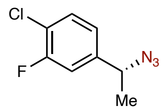

3m[b]
54 ± 3% yield
97:3 e.r.

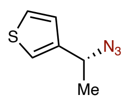

3n
58 ± 1% yield
88.5:11.5 e.r.

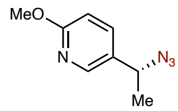

3o
17 ± 1% yield
89.5:10.5 e.r.

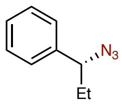

3p[b]
76 ± 1% yield
96:4 e.r.

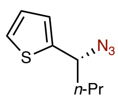

3q[b]
54 ± 1% yield
52:48 e.r.

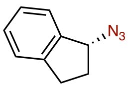

3r[c]
48 ± 1% yield
90:10 e.r.

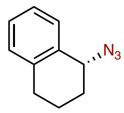

3s[c]
31 ± 1% yield
91:9 e.r.

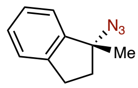

3t
42 ± 3% yield
58:42 e.r.

[a] Reaction conditions: **1** (6.67 mM), **2** (20.0 mM, 3.0 equiv), 1.0 mol% *Pp*MPC I291L L155F F302Y (66.7 μM), 3 mol% fluorescein sodium salt (0.20 mM), 3 mol% $(NH_4)_2Fe(II)(SO_4)_2$ (0.20 mM), *hν* (440 nm), 10 mM HEPES buffer, pH = 7.4, rt, 6 h. [b] 1.0 mol% *Pp*MPC I291L L155F was used in lieu of *Pp*MPC I291L L155F F302Y. [c] 1.0 mol% *Pp*MPC I291L L155F Y255H was used in lieu of *Pp*MPC I291L L155F F302Y. The red sphere is an aryl substituent.

Nonheme Fe enzymes for cooperative photometallobiocata-lytic enantioconvergent decarboxylative thiocyanation

With efficient nonheme enzymes for enantioconvergent radical azidation, we carried out the further engineering of *Pp*MPC to catalyze the asymmetric decarboxylative thiocyanation of redox-active esters (Table 5). In contrast to enantioselective azidation, in the current thiocyanation process, irradiating at 525 nm with green LED provided better results compared to that at 440 nm. Although the nonheme Fe enzyme system showed lower levels of activity towards radical thiocyanation relative to azidation, we found that the *Pp*MPC evolutionary lineage we gathered in the development of catalytic asymmetric azidation described above also showed steady improvement in activity or enantioselectivity for the present catalytic thiocyanation. Specifically, *Pp*MPC I291L displayed a 2.2-fold improvement in activity relative to the wild-type *Pp*MPC (Table 5, entries 1 and 2). The inclusion of L155F to *Pp*MPC I291L substantially enhanced its enantiocontrol over radical thiocyanation, allowing **5a** to form in 42% yield and 94:6 e.r. (entry 3). Starting from *Pp*MPC I291L L155F, an additional round of SSM and screening furnished a new triple mutant *Pp*MPC I291L L155F I204L, allowing the conversion of **(*rac*)-1a** into thiocyanation product **5a** in 54% yield and 95:5 e.r. (entry 4). We note that this isocyanase final variant showed reduced activity and enantioselectivity in azidation reactions. Similarly, the azidation final variant showed inferior activity and enantiocontrol in thiocyanation (entry 5; see Table S10 in the SI for further details).

With the triple mutant radical thiocyanase *Pp*MPC I291L L155F I204L, we briefly surveyed the substrate scope of this dual photobiocatalytic asymmetric radical thiocyanation (Table 6). It was found that secondary alkyl radicals were compatible with this photobiocatalytic protocol. *N*-hydroxyphthalimide esters possessing a methyl group at the *ortho*- (**5b**) and *meta*- (**5c**) positions were converted with excellent enantiocontrol. Substrates with a *para*-chlorine (**5d**) *para*-bromine (**5e**), *meta*-methoxy (**5f**) group as well as a 4-chloro-3-fluoro substrate (**5g**) could also be successfully transformed into the corresponding thiocyanated product with good to excellent levels of enantioselectivity. Moreover, substrates bearing an α-ethyl group

(**5h**) as well as primary benzylic substrates (**5i**) were also readily accommodated by our MPC thiocyanase lineage.

Table 5. Directed evolution of *Pp*MPC for photometallobiocatalytic enantioconvergent decarboxylative thiocyanation of redox-active esters.[a]

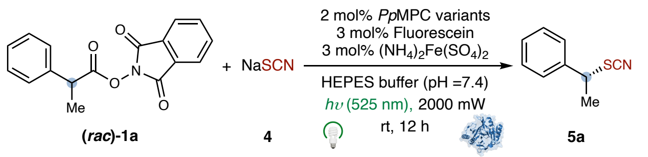

entry	*Pp*MPC variant	yield of **5a**	e.r. of **5a**
1	wt *Pp*MPC	18%	68:32
2	*Pp*MPC I291L	40%	61:39
3	*Pp*MPC I291L L155F	42%	94:6
4	***Pp*MPC I291L L155F I204L (*Pp*MPC thiocyanase)**	**54%**	**95:5**
5	*Pp*MPC I291L L155F F302Y (*Pp*MPC azidase)	22%	**89:11**

[a] Reaction conditions: **1a** (6.67 mM), **4** (66.7 mM, 10.0 equiv), 2.0 mol% PpMPC variant (133.4 mM), 3 mol% fluorescein sodium salt (0.20 mM), 3 mol% $(NH_4)_2Fe(II)(SO_4)_2$ (0.20 mM), *hν* (525 nm), 10 mM HEPES buffer, pH = 7.4, rt, 12 h.

Table 6. Substrate scope of photometallobiocatalytic enantioconvergent decarboxylative thiocyanation of redox-active esters.[a]

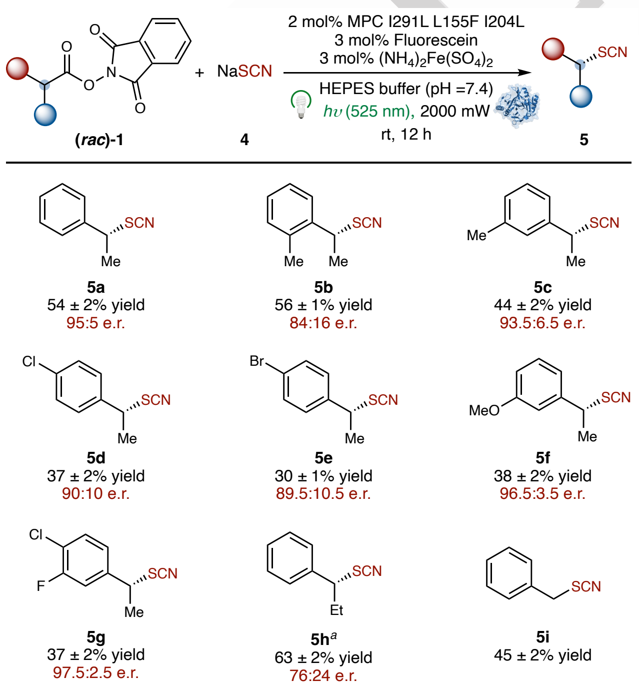

[a] Reaction conditions: **1** (6.67 mM), **4** (66.7 mM, 10.0 equiv), 2.0 mol% *Pp*MPC I291L L155F I204L (133.4 mM), 3 mol% fluorescein sodium salt (0.20 mM), 3 mol% $(NH_4)_2Fe(II)(SO_4)_2$ (0.20 mM), *hν* (525 nm), 10 mM HEPES buffer, pH = 7.4, rt, 6 h. The red sphere is an aryl substituent.

Nonheme Fe enzymes for cooperative photometallobiocatalytic enantioconvergent decarboxylative isocyanation

Having successfully developed nonheme radical azidases and thiocyanases from wt *Pp*MPC, we questioned if our *Pp*MPC variants could also enable the more challenging asymmetric radical isocyanation using NaOCN (**6**) as the inexpensive and abundantly available isocyanating reagent. In contrast to biocatalytic azidation and thiocyanation with nonheme Fe enzymes, enantioselective isocyanation remains largely unexploited within the context of new-to-nature nonheme enzymology. The scarcity of nonheme Fe enzyme-catalyzed isocyanation via a radical rebound mechanism is likely due to the slower lower radical rebound with Fe(III)–NCO as well as the reduced Fe binding affinity of OCN^-.[19b]

To address these limitations, we evaluated our *Pp*MPC azidase and thiocyanase evolutionary lineage for our targeted radical isocyanation reaction. In the early stage of this research, it was found that the radical rebound product alkylisocyanate (R–N=C=O, **7**) underwent rapid hydrolysis in the aqueous buffer. This provided the corresponding alkylamine as the end product, due to the rapid decarboxylation of the carbamic acid resulting from the nucleophilic addition of water to the alkylisocyanate **7**. To circumvent this problem, we evaluated a range of nucleophiles as the trapping reagent to intercept the enzymatically generated enantioenriched organic isocyanate product **7**. After extensive optimization, aniline (**Ph**) was identified as an appropriate isocyanate trapping agent. The appropriate nucleophilicity of aniline allowing the rapid interception of the incipient alkylisocyanate but not the *N*-hydroxyphthalimide ester substrate represented the key to resolving this challenge. Furthermore, using aniline as the trapping agent, this chemoenzymatic cascade afforded unsymmetrical urea product **8** in 20% yield with an excellent enantiomeric ratio of 98:2.

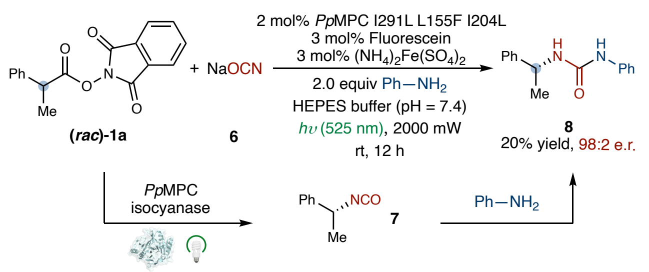

Scheme 2. Photometallobiocatalytic enantioconvergent decarboxylative isocyanation/unsymmetrical urea formation. Reaction conditions: **1a** (6.67 mM), **6** (66.7 mM, 10.0 equiv), aniline (13.3 mM, 2.0 equiv), 2.0 mol% *Pp*MPC I291L L155F I204L (133.4 mM), 3 mol% fluorescein sodium salt (0.20 mM), 3 mol% $(NH_4)_2Fe(II)(SO_4)_2$ (0.20 mM), *hν* (525 nm), 10 mM HEPES buffer, pH = 7.4, rt, 12 h.

Derivatization of organic azides and thiocyanates to access valuable enantioenriched products

To further demonstrate the synthetic utility of our newly developed photometallobiocatalytic enantioconvergent azidation and thiocyanation, we carried out preparative scale enzymatic synthesis and performed downstream transformations to convert organic azide and thiocyanate building blocks into synthetically useful products. Using commercially available Kessil blue LED lamps, the photobiocatalytic azide product **(*R*)-3a** was isolated in 58% yield with 99.5:0.5 e.r.. Starting from **(*R*)-3a**, phosphoramidate **9** and primary amine **11** were obtained in excellent yield and enantiomeric retention via the Staudinger reaction. Additionally, a click reaction with an aryl alkyne afforded the triazole **10** in 83% yield with 99:1 e.r., demonstrating the versatility of the chiral azide compounds[39] Meanwhile, using **(*rac*)-1a**, the thiocyanate product **(*R*)-5a** was generated in 46% yield and 95:5 e.r.. Furthermore, SCF_3[40] derivatives **12** and *S*-tetrazole[41] **13** was obtained in good yield, highlighting the potential for incorporating other functionalities.

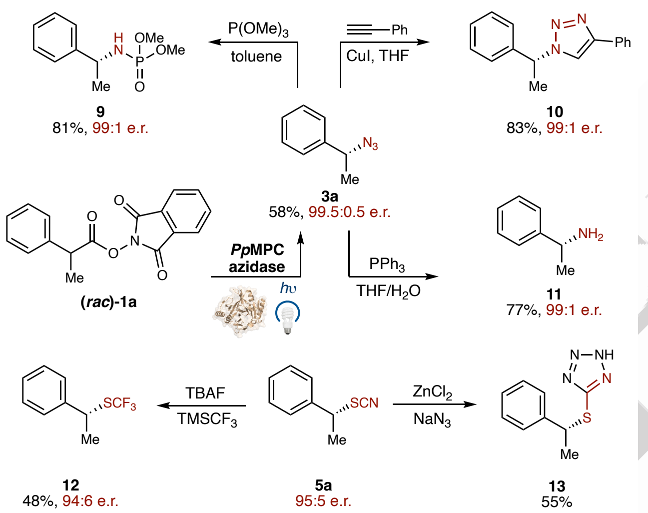

Scheme 3. Derivatization of enantioenriched secondary alkyl azides and thiocyanates.

Computational investigation using DFT and classical MD calculations

To investigate the mechanisms of this nonheme Fe-catalyzed decarboxylative azidation and the origin of enantioselectivity, we performed a combined density functional theory (DFT) and classical molecular dynamics (MD) study. Based on the proposed catalytic cycle (Scheme 1D) and previous mechanistic studies, we surmised that the enantioselectivity-determining step is the radical rebound involving the photoredox-generated prochiral secondary alkyl radical and the Fe(III) azide complex. We performed DFT calculations at the (U)B3LYP-D3/def2-TZVP/SMD(diethyl ether)//(U)B3LYP-D3/SDD(Fe)–6-31G(d) level of theory to study the radical rebound pathways with Fe(III)–N_3 complex **14**, in which the Fe center is coordinated to an acetate as a model for glutamate, two imidazoles (Im) as a model for histidines, a water molecule, and an azide anion. Our DFT calculations indicate that the radical rebound to **14** is highly kinetically facile and exergonic (Figure 2)—the radical addition to the internal nitrogen atom of the Fe(III)–N_3 (**TS1**) requires 1.7 kcal/mol with respect to a van der Waals (vdw) complex (**16**), whereas the radical addition to the terminal nitrogen atom of **14** is barrierless (see Figure S15 for reaction coordinate computed from constrained geometry optimizations). The low barriers suggest that the radical rebound may occur at either the internal or terminal N atom of the nonheme Fe(III)–N_3 in the enzyme active site, depending on the preferred binding poses of the radical. The DFT-optimized transition state structure **TS1** features a long forming C–N bond distance (3.31 Å), indicating an early transition state that is consistent with the high exergonicity. An OH···π interaction[42] between the Fe-bound water and the Ph group on the benzylic radical was observed (3.22 Å) in **TS1**, implying such noncovalent interaction may affect the binding pose of the benzyl radical in the active site. We also computed the radical rebound transition states with a neutral Fe(III) diazide model complex, which require higher barriers for radical rebounds with both internal and terminal azide nitrogen atoms (Figure S13).

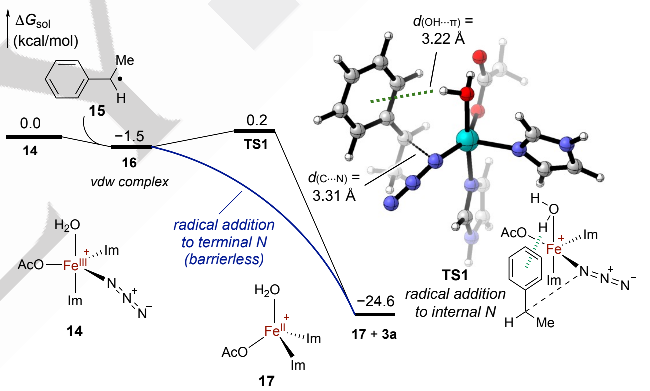

Figure 2. DFT-computed reaction energy profile of the azide radical rebound with a model Fe(III)–N_3 complex **14**. Im = imidazole.

Next, we performed classical MD simulations to study the near-attack conformations (NACs) of the secondary alkyl radical **15** approaching the water-bound Fe(III) azide complex within the active site of *Pp*MPC azidase (*Pp*MPC I291L L155F F302Y) (Figure 3). In these MD simulations, we restrained the forming N–C bond distance between the internal or terminal N of the Fe(III)–N_3 and the benzylic carbon of radical **15** to simulate the NACs of the radical rebound with either the internal or terminal azide N atom. As our engineered *Pp*MPC variants were capable of facilitating both C–S and C–N bond formation from Fe–NCS and Fe–NCO intermediates,[19b] respectively, internal and terminal attack pathways are likely both operative with this nonheme Fe enzyme. We performed 500 ns simulations with the (*Re*)-face of the benzylic radical exposed to the azide to mimic the radical rebound transition state leading to the major (*R*)-enantiomer of the azidation product (see Figure S17 for NAC simulations of azide attacking the (*Si*)-face of the benzylic radical). Our MD simulations revealed that the benzylic radical could adopt various binding poses in the internal and terminal radical rebound pathways, especially when the radical is placed at longer distances from the Fe(III)–N_3 (Figures S21 and S22). In the most favorable binding poses obtained from restrained MD with a relatively short, more product-like, C–N bond distance (Figure 3), the Ph group of the benzylic radical resides in between the nonheme Fe center and the H199 residue, which is *trans* to the E265 residue. The binding pocket *cis* to the E265 residue is blocked by Y255 and Y302 residues, which are connected by a hydrogen bond enabled by the F302Y mutation introduced during directed evolution. The O–H···π interaction between the Fe(III)-bound water and the Ph group on the radical was observed, although the O–H···π distance from the MD trajectories is longer than that in DFT-optimized structure, because the Ph group is also involved in π···π interaction with H153. This radical rebound geometry is consistent with the experimentally observed enantioinduction—when the (*Re*)-face of the benzylic radical is exposed to the azide, the smallest substituent H on the secondary benzylic radical is placed towards the relatively hindered L155F residue, whereas the (*Si*)-face radical addition is expected to be disfavored due to steric repulsions between the Me substituent on the benzylic carbon and L155F (see Figures S18–S20). This enantioinduction model is consistent with the experimentally observed increased enantioselectivity with the L155F and F302Y mutations.

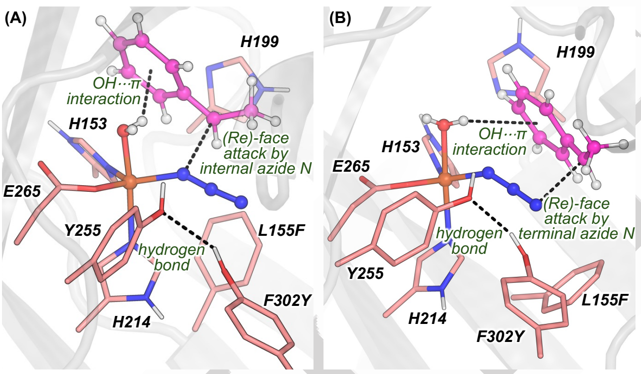

Figure 3. Representative structures from 500 ns MD simulations of the near-attack conformations (NAC) that expose the (*Re*)-face of the benzylic radical **15** (shown in purple) to the Fe(III)–N_3 intermediate. The forming C–N bond distance with the (A) internal and (B) terminal azide N atoms was restrained. Key active site residues around the azide and the alkyl radical are shown in pink. See Figures S21 and S22 for radical binding poses at longer forming C–N bond distances.

Conclusions

In conclusion, through the cooperative interactions between an engineered nonheme Fe enzyme and a carefully selected photocatalyst, we developed dual photometallobiocatalytic decarboxylative radical azidation, thiocyanation and isocyanation of redox-active *N*-hydroxyphthalimide esters. Mechanistically, a radical rebound step involving nonheme enzymatic Fe(III)–N_3, Fe(III)–NCS and Fe(III)–NCO intermediates represented the unifying mechanism underlying these transformations. The evaluation of an in-house collection of nonheme Fe enzymes allowed the identification of several promising starting points for the development of photometallobiocatalytic radical transformations. In particular, metapyrocatechase (MPC), a nonheme Fe extradiol dioxygenase which has not been studied in prior new-to-nature biocatalysis research, was identified as an excellent biocatalyst. Enabled by high-throughput photobiocatalysis, further directed evolution led to MPC triple variants with substantially improved activity and enantioselectivity for azidation, thiocyanation and isocyanation. These evolved MPC variants allowed an array of primary, secondary and tertiary radical precursors to be transformed, leading to useful products with excellent enantioselectivity. Further chemical derivatization of these C–N and C–S bond forming products demonstrated the synthetic utility of these chiral building blocks. Computational studies afforded further insights into the mechanism and origin of enantioselectivity in the present nonheme photobiocatalysis. An enantioinduction model was proposed based on MD simulations of the alkyl radical approaching the Fe(III)–N_3 in the enzyme active site, where the F302Y and L155F mutations introduced in directed evolution play important roles in affecting the preferred binding poses and the orientation of the prochiral radical intermediate prior to the enantiodetermining radical rebound. Overall, engineered nonheme Fe enzyme MPC and related extradiol dioxygenase may find broader applications in other non-native biocatalytic reaction. We expect the use of cooperative photobiocatalysis to inspire the further development of a wider range of synthetically useful transformations catalyzed by nonheme Fe enzymes.

Acknowledgements

The experimental research described herein is supported by the NIH (R35GM147387 to Y.Y.). The computational research described herein is supported by the NSF (CHE-2400087). Y.Y. is an Alfred P. Sloan Research Fellow, a Camille Dreyfus Teacher-Scholar Awardee and a David & Lucile Packard Fellowship Awardee. We acknowledge the NSF BioPACIFIC MIP (DMR-1933487) and NSF MRSEC at UCSB (DMR-2308708) for access to instrumentation. Molecular dynamics simulations were performed at the Center for Research Computing of the University of Pittsburgh and the Advanced Cyberinfrastructure Coordination Ecosystem: Services & Support (ACCESS) program supported by the National Science Foundation grant numbers OAC-2117681 and OAC-2138259.

Keywords: photometallobiocatalysis • enzymes • iron • reaction mechanisms • synthetic methods

[1] For recent reviews: a) K. Chen, F. H. Arnold, *Nat. Catal.* **2020**, *3*, 203-213. b) R. Buller, S. Lutz, R. J. Kazlauskas, R. Snajdrova, J. C. Moore, U. T. Bornscheuer, *Science* **2023**, *382*, eadh8615. c) S. Jain, F. Ospina, S. C. Hammer, *JACS Au* **2024**, *4*, 2068-2080.

[2] For reviews on radical biocatalysis with ketoreductases (KREDs) and ene reductases (EREDs): a) W. Harrison, X. Huang, H. Zhao, *Acc. Chem. Res.* **2022**, *55*, 1087-1096. b) M. A. Emmanuel, S. G. Bender, C. Bilodeau, J. M. Carceller, J. S. DeHovitz, H. Fu, Y. Liu, B. T. Nicholls, Y. Ouyang, C. G. Page, T. Qiao, F. C. Raps, D. R. Sorigue, S. Z. Sun, J. Turek-Herman, Y. Ye, A. Rivas-Souchet, J. Cao, T. K. Hyster, *Chem. Rev.* **2023**, *123*, 5459-5520. c) H. Fu, T. K. Hyster, *Acc. Chem. Res.* **2024**, *57*, 1446-1457. d) J. Yu, B. Chen, X. Huang, *Angew. Chem. Int. Ed.* **2024**, e202419262.

[3] Imine reductase (IRED) repurposing: B. Chen, R. Li, J. Feng, B. Zhao, J. Zhang, J. Yu, Y. Xu, Z. Xing, Y. Zhao, B. Wang, X. Huang, *J. Am. Chem. Soc.* **2024**, *146*, 14278–14286.

[4] Fatty acid photodecarboxylase (FAP) repurposing: a) S. Ju, D. Li, B. K. Mai, X. Liu, A. Vallota-Eastman, J. Wu, D. L. Valentine, P. Liu, Y. Yang, *Nat. Chem.* **2024**, *16*, 1339-1347. b) W. Xu, K. Mou, Z. Lu, X. Kang, Y. Guo, B. Ding, Z. Chen, Z. Wang, Q. Wu, *Angew. Chem. Int. Ed.* **2024**, *63*, e202412862.

[5] Cyclohexanone monooxygenase (CHMO) repurposing: a) Y. Peng, Z. Wang, Y. Chen, W. Xu, Y. Hu, Z. Chen, J. Xu, Q. Wu, *Angew. Chem. Int. Ed.* **2022**, *61*, e202211199. b) F. C. Raps, A. Rivas-Souchet, C. M. Jones, T. K. Hyster, *Nature* **2024**, 10.1038/s41586-41024-08138-w.

[6] Pyridoxal 5'-phosphate (PLP) enzyme repurposing: a) L. Cheng, D. Li, B. K. Mai, Z. Bo, L. Cheng, P. Liu, Y. Yang, *Science* **2023**, *381*, 444-451. b) T.-C. Wang, B. K. Mai, Z. Zhang, Z. Bo, J. Li, P. Liu, Y. Yang, *Nature* **2024**, *629*, 98-104. c) T.-C. Wang, Z. Zhang, G. Rao, J. Li, J. Shirah, R. D. Britt, Q. Zhu, Y. Yang, *J. Am. Chem. Soc.* **2024**, *146*, 22476-22484. d) Y. Ouyang, C. G. Page, C. Bilodeau, T. K. Hyster, *J. Am. Chem. Soc.* **2024**, *146*, 13754-13759.

[7] Thiamine pyrophosphate (TPP) enzyme repurposing: a) Y. Xu, H. Chen, L. Yu, X. Peng, J. Zhang, Z. Xing, Y. Bao, A. Liu, Y. Zhao, C. Tian, *Nature* **2024**, *625*, 74-78. b) X. Liu, S. Xu, H. Chen, Y. Yang, *ACS Catal.* **2024**, *14*, 9144-9150. c) Z. Xing, F. Liu, J. Feng, L. Yu, Z. Wu, B. Zhao, B. Chen, H. Ping, Y. Xu, A. Liu, Y. Zhao, C. Wang, B. Wang, X. Huang, *Nature* **2024**, *2024*, 10.1038/s41586-41024-08399-41585.

[8] P450 halogen atom transferases: a) Q. Zhou, M. Chin, Y. Fu, P. Liu, Y. Yang, *Science* **2021**, *374*, 1612-1616. b) Y. Fu, H. Chen, W. Fu, M. Garcia-Borràs, Y. Yang, P. Liu, *J. Am. Chem. Soc.* **2022**, *144*, 13344-13355. c) W. Fu, N. M. Neris, Y. Fu, Y. Zhao, B. Krohn-Hansen, P. Liu, Y. Yang, *Nat. Catal.* **2023**, *6*, 628-636. d) W. Fu, Y. Fu, Y. Zhao, H. Wang, P. Liu, Y. Yang, *Nat. Chem.* **2024**, *16*, 1999-2008.

[9] Nonheme Fe (pseudo)halogen transferases: a) J. Rui, Q. Zhao, A. J. Huls, J. Soler, J. C. Paris, Z. Chen, V. Reshetnikov, Y. Yang, Y. Guo, M. Garcia-Borràs, X. Huang, *Science* **2022**, *376*, 869-874. b) Q. Zhao, Z. Chen, J. Soler, X. Chen, J. Rui, N. T. Ji, Q. E. Yu, Y. Yang, M. Garcia-Borràs, X. Huang, *Nat. Synth.* **2024**, *3*, 958-966. c) L.-P. Zhao, B. K. Mai, L. Cheng, F. Gao, Y. Zhao, R. Guo, H. Wu, Y. Zhang, P. Liu, Y. Yang, *Nat. Synth.* **2024**, *3*, 967-975. d) J. G. Zhang, A. J. Huls, P. M. Palacios, Y. Guo, X. Huang, *J. Am. Chem. Soc.* **2024**, *146*, 34878-34886.

[10] For related Zn/Fe enzyme-catalyzed hydride transfer processes that may not involve a radical mechanism: a) P. Ji, J. Park, Y. Gu, D. S. Clark, J. F. Hartwig, *Nat. Chem.* **2021**, *13*, 312-318. b) R. Chen, C. S. Kayrouz, E. McAmis, D. S. Clark, J. F. Hartwig, *Angew. Chem. Int. Ed.* **2024**, *63*, e202407111. c) X. Zhang, D. Chen, J. Stropp, R. Tachibana, Z. Zou, D. Klose, T. R. Ward, *Chem* **2024**, *10*, 2577-2589.

[11] J. Li, A. Kumar, J. C. Lewis, *Angew. Chem. Int. Ed.* **2023**, *62*, e202312893.

[12] For reviews on stereoselective radical reactions: a) M. P. Sibi, S. Manyem, J. Zimmerman, *Chem. Rev.* **2003**, *103*, 3263-3296. b) R. S. Proctor, A. C. Colgan, R. J. Phipps, *Nat. Chem.* **2020**, *12*, 990-1004. c) S. Mondal, F. Dumur, D. Gigmes, M. P. Sibi, M. P. Bertrand, M. Nechab, *Chem. Rev.* **2022**, *122*, 5842-5976.

[13] a) M. A. Emmanuel, N. R. Greenberg, D. G. Oblinsky, T. K. Hyster, *Nature* **2016**, *540*, 414-417. b) K. F. Biegasiewicz, S. J. Cooper, X. Gao, D. G. Oblinsky, J. H. Kim, S. E. Garfinkle, L. A. Joyce, B. A. Sandoval, G. D. Scholes, T. K. Hyster, *Science* **2019**, *364*, 1166-1169. c) C. G. Page, S. J. Cooper, J. S. DeHovitz, D. G. Oblinsky, K. F. Biegasiewicz, A. H. Antropow, K. W. Armbrust, J. M. Ellis, L. G. Hamann, E. J. Horn, *J. Am. Chem. Soc.* **2020**, *143*, 97-102.

[14] For reviews on photoredox catalysis: a) J. M. Narayanam, C. R. Stephenson, *Chem. Soc. Rev.* **2011**, *40*, 102-113. b) C. K. Prier, D. A. Rankic, D. W. MacMillan, *Chem. Rev.* **2013**, *113*, 5322-5363. c) K. L. Skubi, T. R. Blum, T. P. Yoon, *Chem. Rev.* **2016**, *116*, 10035-10074. d) N. A. Romero, D. A. Nicewicz, *Chem. Rev.* **2016**, *116*, 10075-10166.

[15] α-Ketoglutarate-dependent nonheme Fe halogenases: a) F. H. Vaillancourt, J. Yin, C. T. Walsh, *Proc. Natl. Acad. Sci. U.S.A.* **2005**, *102*, 10111-10116. b) L. C. Blasiak, F. H. Vaillancourt, C. T. Walsh, C. L. Drennan, *Nature* **2006**, *440*, 368-371. c) M. L. Hillwig, X. Liu, *Nat. Chem. Biol.* **2014**, *10*, 921-923. d) A. J. Mitchell, Q. Zhu, A. O. Maggiolo, N. R. Ananth, M. L. Hillwig, X. Liu, A. K. Boal, *Nat. Chem. Biol.* **2016**, *12*, 636-640. e) T. Hayashi, M. Ligibel, E. Sager, M. Voss, J. Hunziker, K. Schroer, R. Snajdrova, R. Buller, *Angew. Chem. Int. Ed.* **2019**, *58*, 18535-18539. f) J. A. Marchand, M. E. Neugebauer, M. C. Ing, C. I. Lin, J. G. Pelton, M. C. Y. Chang, *Nature* **2019**, *567*, 420-424. g) M. E. Neugebauer, K. H. Sumida, J. G. Pelton, J. L. McMurry, J. A. Marchand, M. C. Y. Chang, *Nat. Chem. Biol.* **2019**, *15*, 1009-1016. h) S. Duewel, L. Schmermund, T. Faber, K. Harms, V. Srinivasan, E. Meggers, S. Hoebenreich, *ACS Catal.* **2020**, *10*, 1272-1277. i) C. Y. Kim, A. J. Mitchell, C. M. Glinkerman, F.-S. Li, T. Pluskal, J.-K. Weng, *Nat. Commun.* **2020**, *11*, 1867. j) C. Zhao, S. Yan, Q. Li, H. Zhu, Z. Zhong, Y. Ye, Z. Deng, Y. Zhang, *Angew. Chem. Int. Ed.* **2020**, *59*, 9478-9484. k) J. Büchler, S. H. Malca, D. Patsch, M. Voss, N. J. Turner, U. T. Bornscheuer, O. Allemann, C. Le Chapelain, A. Lumbroso, O. Loiseleur, R. Buller, *Nat. Commun.* **2022**, *13*, 371. l) M. E. Neugebauer, E. N. Kissman, J. A. Marchand, J. G. Pelton, N. A. Sambold, D. C. Millar, M. C. Y. Chang, *Nat. Chem. Biol.* **2022**, *18*, 171-179. m) M. Voss, S. Hüppi, D. Schaub, T. Hayashi, M. Ligibel, E. Sager, K. Schroer, R. Snajdrova, R. Buller, *ChemCatChem* **2022**, *14*, e202201115. n) E. N. Kissman, M. E. Neugebauer, K. H. Sumida, C. V. Swenson, N. A. Sambold, J. A. Marchand, D. C. Millar, M. C. Y. Chang, *Proc. Natl. Acad. Sci. U.S.A.* **2023**, *120*, e2214512120. o) J. Ni, J. Zhuang, Y. Shi, Y.-C. Chiang, G.-J. Cheng, *Nat. Commun.* **2024**, *15*, 5254-5266. p) A. J. Mitchell, N. P. Dunham, J. A. Bergman, B. Wang, Q. Zhu, W.-c. Chang, X. Liu, A. K. Boal, *Biochemistry* **2017**, *56*, 441-444.

[16] a) M. L. Matthews, W.-c. Chang, A. P. Layne, L. A. Miles, C. Krebs, J. M. Bollinger, *Nat. Chem. Biol.* **2014**, *10*, 209-215. b) C. A. Gomez, D. Mondal, Q. Du, N. Chan, J. C. Lewis, *Angew. Chem. Int. Ed.* **2023**, *62*, e202301370. c) N. H. Chan, C. A. Gomez, V. Vennelakanti, Q. Du, H. J. Kulik, J. C. Lewis, *Inorg. Chem.* **2022**, *61*, 14477-14485.

[17] a) M. Quareshy, M. Shanmugam, E. Townsend, E. Jameson, T. D. H. Bugg, A. D. Cameron, Y. Chen, *J. Biol. Chem.* **2021**, *296*, 100038. b) M. Quareshy, M. Shanmugam, A. D. Cameron, T. D. H. Bugg, Y. Chen, *FEBS J.* **2023**, *290*, 2939-2953.

[18] For a review on nonheme Fe halogenases: A. Papadopoulou, F. Meyer, R. M. Buller, *Biochemistry* **2023**, *62*, 229-240.

[19] a) V. Yadav, L. Wen, R. J. Rodriguez, M. A. Siegler, D. P. Goldberg, *J. Am. Chem. Soc.* **2022**, *144*, 20641-20652. b) V. Yadav, L. Wen, S. Yadav, M. A. Siegler, D. P. Goldberg, *Inorg. Chem.* **2023**, *62*, 17830-17842. c) E. F. Gérard, V. Yadav, D. P. Goldberg, S. P. de Visser, *J. Am. Chem. Soc.* **2022**, *144*, 10752-10767. d) A. Y. Chan, I. B. Perry, N. B. Bissonnette, B. F. Buksh, G. A. Edwards, L. I. Frye, O. L. Garry, M. N. Lavagnino, B. X. Li, Y. Liang, E. Mao, A. Millet, J. V. Oakley, N. L. Reed, H. A. Sakai, C. P. Seath, D. W. C. MacMillan, *Chem. Rev.* **2022**, *122*, 1485-1542.

[20] a) P. Sivaguru, Y. Ning, X. Bi, *Chem. Rev.* **2021**, *121*, 4253-4307. b) A. Sharma, J. F. Hartwig, *Nature* **2015**, *517*, 600-604. c) R. R. Karimov, A. Sharma, J. F. Hartwig, *ACS Cent. Sci.* **2016**, *2*, 715-724. d) C. S. Day, A. Fawcett, R. Chatterjee, J. F. Hartwig, *J. Am. Chem. Soc.* **2021**, *143*, 16184-16196. e) W. Liu, M. Pu, J. He, T. Zhang, S. Dong, X. Liu, Y.-D. Wu, X. Feng, *J. Am. Chem. Soc.* **2021**, *143*, 11856-11863. f) L. Ge, H. Zhou, M.-F. Chiou, H. Jiang, W. Jian, C. Ye, X. Li, X. Zhu, H. Xiong, Y. Li, L. Song, X. Zhang, H. Bao, *Nat. Catal.* **2021**, *4*, 28-35. g) L. Ge, H. Wang, Y. Liu, X. Feng, *J. Am. Chem. Soc.* **2024**, *146*, 13347-13355.

[21] a) F. Wang, P. Chen, G. Liu, *Acc. Chem. Res.* **2018**, *51*, 2036-2046. b) X. Wang, J. He, Y.-N. Wang, Z. Zhao, K. Jiang, W. Yang, T. Zhang, S. Jia, K. Zhong, L. Niu, Y. Lan, *Chem. Rev.* **2024**, *124*, 10192-10280.

[22] a) F. Buttard, J. Vigier, H. Lebel, T. Besset, *Eur. J. Org. Chem.* **2024**, *27*, e202301205. b) C. Jiang, P. Chen, G. Liu, *CCS Chem.* **2021**, *3*, 1884-1893.

[23] S.-E. Suh, L. E. Nkulu, S. Lin, S. W. Krska, S. S. Stahl, *Chem. Sci.* **2021**, *12*, 10380-10387.

[24] T. Shen, Z.-G. Zhao, Q. Yu, H.-J. Xu, *J. Photochem. Photobiol., A* **1989**, *47*, 203-212.

[25] The native reaction catalyzed by extradiol dioxygenase MPC is shown below:

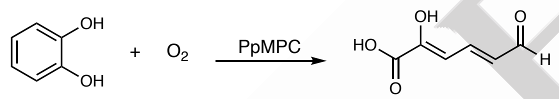

a) A. Kita, S.-i. Kita, I. Fujisawa, K. Inaka, T. Ishida, K. Horiike, M. Nozaki, K. Miki, *Structure* **1999**, *7*, 25-34. b) T. Ishida, A. Kita, K. Miki, M. Nozaki, K. Horiike, in *Int. Congr. Ser., Vol. 1233*, **2002**, pp. 213-220.

[26] J. Rui, X. Mu, J. Soler, J. C. Paris, Y. Guo, M. Garcia-Borràs, X. Huang, *Nat. Catal.* **2024**, *7*, 1394-1403.

[27] P. Liu, K. Murakami, T. Seki, X. He, S.-M. Yeung, T. Kuzuyama, H. Seto, H.-w. Liu, *J. Am. Chem. Soc.* **2001**, *123*, 4619-4620.

[28] J. M. Brownlee, K. Johnson-Winters, D. H. Harrison, G. R. Moran, *Biochemistry* **2004**, *43*, 6370-6377.

[29] L. Bowater, S. A. Fairhurst, V. J. Just, S. Bornemann, *FEBS Lett.* **2004**, *557*, 45-48.

[30] a) Z. Zhang, J.-S. Ren, I. J. Clifton, C. J. Schofield, *Chem. Biol.* **2004**, *11*, 1383-1394. b) M. Houben, B. Van de Poel, *Front. Plant Sci.* **2019**, *10*, 695.

[31] A. Kitayama, T. Achioku, T. Yanagawa, K. Kanou, M. Kikuchi, H. Ueda, E. Suzuki, H. Nishimura, T. Nagamune, Y. Kawakami, *J. Ferment. Bioeng.* **1996**, *82*, 217-223.

[32] a) F. P. Seebeck, *J. Am. Chem. Soc.* **2010**, *132*, 6632-6633. b) K. V. Goncharenko, A. Vit, W. Blankenfeldt, F. P. Seebeck, *Angew. Chem. Int. Ed.* **2015**, *54*, 2821-2824.

[33] S. Fukuzumi, H. Kotani, K. Ohkubo, S. Ogo, N. V. Tkachenko, H. Lemmetyinen, *J. Am. Chem. Soc.* **2004**, *126*, 1600-1601.

[34] T. Qin, J. Cornella, C. Li, L. R. Malins, J. T. Edwards, S. Kawamura, B. D. Maxwell, M. D. Eastgate, P. S. Baran, *Science* **2016**, *352*, 801-805.

[35] E. P. Chovancova, A.; Benes, P.; Strnad, O.; Brezovsky, J.; Kozlikova, B.; Gora, A.; Sustr, V.; Klvana, M.; Medek, P.; Biedermannova, L.; Sochor, J.; Damborsky, J., *PLoS Comput. Biol.* **2012**, *8*, e1002708.

[36] T. Kobayashi, T. Ishida, K. Horiike, Y. Takahara, N. Numao, A. Nakazawa, T. Nakazawa, M. Nozaki, *J. Biochem.* **1995**, *117*, 614-622.

[37] S. Kille, C. G. Acevedo-Rocha, L. P. Parra, Z.-G. Zhang, D. J. Opperman, M. T. Reetz, J. P. Acevedo, *ACS synthetic biology* **2013**, *2*, 83-92.

[38] E.-i. Negishi, in *Handbook of Organopalladium Chemistry for Organic Synthesis*, John Wiley&Sons, **2002**.

[39] S. Bräse, C. Gil, K. Knepper, V. Zimmermann, *Angew. Chem. Int. Ed.* **2005**, *44*, 5188-5240.

[40] X.-H. Xu, K. Matsuzaki, N. Shibata, *Chem. Rev.* **2015**, *115*, 731-764.

[41] C. G. Neochoritis, T. Zhao, A. Domling, *Chem. Rev.* **2019**, *119*, 1970-2042.

[42] a) S. Suzuki, P. G. Green, R. E. Bumgarner, S. Dasgupta, W. A. Goddard, G. A. Blake, *Science* **1992**, *257*, 942-945. b) S. Tsuzuki, K. Honda, T. Uchimaru, M. Mikami, K. Tanabe, *J. Am. Chem. Soc.* **2000**, *122*, 11450-11458.

Entry for the Table of Contents

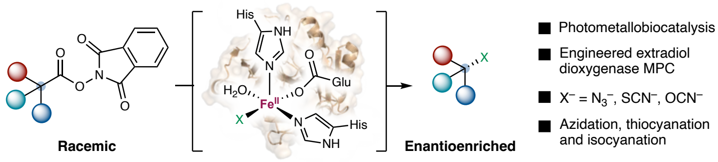

Through the directed evolution of an underexploited nonheme Fe extradiol dioxygenase, we developed a unified cooperative photobiocatalytic strategy to allow for three types of enantioconvergent radical transformations, including azidation, thiocyanation and isocyanation. Computational studies based on density functional theory (DFT) and molecular dynamics (MD) simulations suggested a π-facial selective radical rebound mechanism as the enantiodetermining step.

Institute and/or researcher Twitter usernames: @yang2biocat